A Low-Power RFID Integrated Circuits for Intelligent Healthcare Systems

Shuenn-Yuh Lee, *Member, IEEE*, Liang-Hung Wang, *Student Member, IEEE*, and Qiang Fang, *Member, IEEE*

Abstract—This paper presents low-power radio-frequency identification (RFID) technology for intelligent healthcare systems. With attention to power-efficient communication in the body sensor network, RF power transfer was estimated and the required low-power ICs, which are important in the development of a healthcare system with miniaturization and system integration, are discussed based on the RFID platform. To analyze the power transformation, this paper adopts a 915-MHz industrial, scientific, and medical RF with a radiation power of 70 mW to estimate the power loss under the 1-m communication distance between an RFID reader (bioinformation node) and a transponder (biosignal acquisition nodes). The low-power ICs of the transponder will be implemented in the TSMC 0.18-μm CMOS process. The simulation result reveals that the transponder's IC can fit in with the link budget of the UHF RFID system.

Index Terms—Body sensor network, bioinformation, biosignal acquisition, healthcare, low-power, radio-frequency identification (RFID), reader, transponder.

I. INTRODUCTION

HEALTHCARE monitoring using radio-frequency identification (RFID) technology is predicted as the next stage in home care due to its great potential as a low-cost and high patient-safety medical service [1], [2]. In recent years, the ergonomics industry has invested more money into the development of information technology engineering (ITE) to improve patient safety and enhance nursing efficiency, in addition to decreasing healthcare expenses. The RFID system is expected to be a good choice for healthcare organizations to achieve the objective [3].

RFID technology transfers the healthcare monitoring from the clinic to the home-health center for long-term attention. Generally, home-based monitoring allows patients to examine their own situations in their normal daily activities using the biosignal acquisition node (BAN) [4], [5]. In the body sensor network, the bioinformation is collected in the reader and the message can be submitted to the healthcare center by the local sensor network for diagnosis. Moreover, if a patient is leaving the healthcare center without permission, the RFID system can also send an alarm to the healthcare center to avoid any possible problems. This function is especially important for the healthcare of elders.

Three main parts compose an RFID system: 1) an RFID transponder (called a tag) with an antenna and an information-storage chip that can sense the biosignal and transit the information to an off-chip reader; 2) an RFID reader, which can simultaneously read and write (program or erase) on several transponders without the line of sight; and 3) a data-control system used to handle the received/transmitted information between the reader and the transponders.

There are two main types of RFID transponders namely, active and passive transponders. Active transponders have a greater potential to achieve a more stable transmission, although its size is larger and requires battery power. In contrast, the advantages of passive transponders include its smaller size, absence of power requirement, greater flexibility, simplicity, and long-term operation capacity. However, passive transponders are limited in terms of the resolution of location and short reading distance. Since long-term operation dominates healthcare applications, the passive RFID transponder is preferred in healthcare monitoring and medication management.

Traditionally, LF and HF passive transponders with coils as antennas operated at 125 kHz and 13.56 MHz, respectively, have been widely used in RFID products under near-field communication (NFC). However, using LF and HF communication for wearable healthcare monitoring systems will result in some problems: 1) lower efficiency because of the bigger antennas with lower frequency capability; and 2) short reading distance, typically, the communicated distances are limited to less than 20 cm by coils antenna coupling in NFC. Due to the demands for higher data rates, longer reading distances, and smaller antenna sizes, people will be more interested in the UHF 868/915-MHz or microwave 2.4-GHz industrial, scientific, and medical (ISM) bands. However, more popular wireless communication systems have been allocated in microwave 2.4-GHz ISM band, including wireless LAN (WLAN: 802.11 b) and wireless personal area network (WPAN: Bluetooth and ZigBee). Table I illustrates the comparison of properties between 802.11 b, Bluetooth, ZigBee, and RFID systems. It reveals that the selected UHF 868/915-MHz in RFID design is preferred for healthcare systems to avoid the influences of WLAN and WPAN.

This paper seeks to estimate the power transformation in the UHF band, i.e., 915 MHz, between the reader and the

TABLE I
WIRELESS STANDARD IN ISM BAND

Features	802.11 b	Bluetooth	ZigBee	RFID
Power Profile	Hours	Days	Years	Batteryless
Complexity	Very Complex	Complex	Simple	Simple
Nodes/Master	32	7	6400	100
Modulation	QPSK	FSK, GMSK	BPSK, O-QPSK	ASK, PSK
Range	100 m	10 m	10 m	10cm ~ 10 m
Frequency	2.45 GHz	2.45 GHz	2.45 GHz	LF, HF, UHF
Data Rate	11 Mbps	1 Mbps	250 kbps	64 kbps
Security	802.1x	64 bit, 128 bit	AES-128bit	EPC-GEN II

transponder. A transponder with the capability for ac-power rectification, a system clock generation, a dc-voltage regulation, an ASK demodulation/modulation, digital control, and biosignal acquisition is simulated and the power consumption of the whole system is estimated. The circuit simulation and device modeling of a 0.18-μm RF CMOS standard process are adopted to demonstrate that low-voltage low-power ICs are well suited for the requirement of the power transformation in a UHF band.

In Section II, a healthcare monitoring system is introduced. Section III describes the methodology of the estimation of the RFID power consumption, including the near and far fields, which are relative to the operated bands of RFID systems, and the power transmission between transmitted reader and received transponder. In Section IV, the circuit implementation of the passive RFID transponders is presented. Moreover, the power consumption of the circuits in each block is also estimated by the circuit simulator, HSPICE. The estimation results and conclusion are presented in Section V.

II. HEALTHCARE MONITORING SYSTEM

With aging population, it has also grown many chronic diseases, simultaneously. People should face up to this phenomenon and discover the required solution. Prevention is better than cure, and it is an important concept in the current society. In recent years, home telecare system (HTS) has been employed for self-examination and biosignal transmission between person and medical center by Internet or wireless communication systems [6]–[9]. However, the HTS is not a mobile observation system of anytime and anywhere for elders and patients. In order to enhance the portability and increase the popularization of HTS, an interactive intelligent healthcare and monitoring system (IIHMS) is proposed, as shown in Fig. 1.

Conventional healthcare monitoring can be divided into two phases. The first phase is the treatment in the hospital, the most urgent and the shortest medical therapy. If patients are ill, they go to the hospital to receive emergency diagnosis and treatment. The second phase is the long-time medical care in the healthcare center, which incurs a bigger social cost because more human power and expensive medication are required to take care of patients. To economize on the social cost and improve the quality of medical treatment, a platform capable of examination anywhere and anytime by itself should be developed, which can transmit personal examination data to the healthcare center or hospital via the Internet or wireless application

systems [6]. Fig. 1 illustrates the concept of IIHMS via heterogeneous networks, including the body sensor network and local sensor network [7]–[10]. The body sensor network is used for communication between the BANs and bioinformation node (BIN), and the personal examination data can be transmitted to the bioaware service gateway (BGate) via the local sensor network, such as the ZigBee sensor network for diagnosis. The details are described in the next sections.

A. Body Sensor Network

The body sensor network provides the communication between the BANs and the BIN with RFID technology at 915 MHz. The BANs include the biosignal acquisition circuits and RF front-end circuits for transmitting the multibiosignals to the BIN. To miniaturize the sensor nodes (BANs), a system-on-a-chip (SOC) with very large-scale integration (VLSI) technology should be employed in the circuit implementation. Moreover, for the permanent and portable requirements, a passive RF transceiver circuit that does not rely on a battery, as well as a low-power analog acquisition circuit, should be developed. The BIN is similar to a reader of the RFID that can be embedded in an RFID mobile phone or an RFID watch. It can receive the encryption security data from the BANs through the body sensor network. Power-conversion efficiency (PCE), accurate data transmission, and microwave radiation are the major considerations in the body sensor network. However, the ability of noise resistance is another problem in body sensor network. The biosignal is usually difficult to be acquired because people moving or environment changing will result in low SNR. Therefore, the noise tolerance should also be considered in low-power analog signal processing.

B. Local Sensor Network

The local sensor network shown in Fig. 1 supports the communication medium between the BIN and BGate for biosignal analysis and biocontext-aware service. Aside from this, the power-transmission efficiency and the data-transmission quality can be improved by this interactive network. However, the personal examination data should be encrypted to assure the highest confidentiality when the data are communicated between the BIN and BGate. Moreover, the BGate holds an important communication bridge between the human body and the network server. It not only supplies the service of health monitoring, but also conveys the advices of doctor for patients. If disease diagnosis is required, the data in the BGate can further be submitted to the healthcare center or hospital via the Internet or other telecommunication channels [11]–[13].

C. Intelligent Healthcare Service

Fig. 2 shows an example of ECG signal acquisition and processing flow. First, the ECG signal is acquired from the cardiopathy electrode leads. To enhance the SNR, the recorded signals should be amplified, filtered, and digitized before transmission to the BIN by the RFID transmitter. Therefore, a preamplifier, a filter, an AD converter (ADC), and a class-E amplifier with ASK
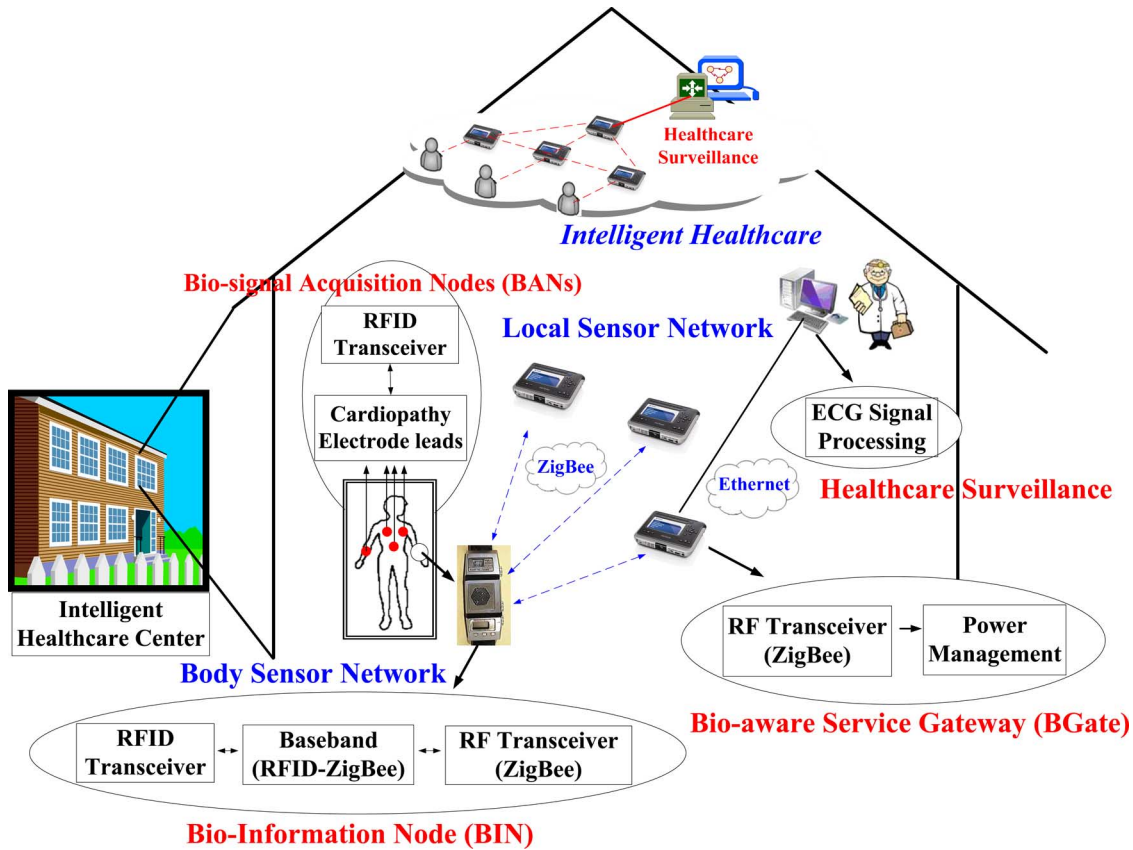
Fig. 1.   Heterogeneous networks for healthcare monitoring.

modulation are required in the sensing path. The required supply voltage of the described analog ICs would be extracted from the RFID receiver according to the on-chip rectifier and regulator. Furthermore, the ECG signal can be received by the BIN, which likewise performs data verification and encryption. This assures the highest confidentiality and prevents data interference by other devices [14], [15]. The aforementioned procedure is accomplished in the body sensor network.

The local sensor network system is the communication medium between the BIN and the BGate. The received data in the BGate will be verified and decrypted by the ECG server and analyzed by the healthcare center and doctor. If the server finds a seriously abnormal ECG signal, the healthcare center will send the emergency message to the hospital nearest to the patient so that urgent medical service can be provided. Moreover, the doctor in the clinic (doctor node) can periodically check the person's ECG signal to diagnose any abnormality in advance.

III. RFID POWER ESTIMATION

A. RFID Field Analysis

In RFID application, the space between the reader and antenna of transponder can be divided into two main regions: the near-field region and the far-field region, as illustrated in Fig. 3 [16].

1) Near-Field Region: It includes two subregions: a radiating region where the angular field distribution is dependent on the distance, and a reactive region where the energy is stored, but not radiated. In the near-field region, the coil antenna with inductively coupled magnetic field H is employed to transmit the RF power and biosignal. Fig. 4 shows the path of the lines of magnetic flux around a short round coil. Equation (1) can be used to calculate the field strength H along the X-axis of a round coil, where N is the number of windings, R is the coil radius, and r is the distance between the radiated source and the received object in X-axis direction

$$H = \frac{INR^2}{2\sqrt{(R^2 + r^2)^3}}. \tag{1}$$

The wave radiation distance is dependent on the different angular and transmission media, and the radiation attenuation via free-space impedance is approximately decayed by $1/r^3$.

2) Far-Field Region: The wave-propagation patterns cover the electric and magnetic fields outward as orthogonal and direction radiation electromagnetic (EM) wave. The energy transported by the EM wave is stored in the electric and magnetic field of the wave. The power-radiation density $\overrightarrow{S}$ can be found from the Poynting radiation vector $\overrightarrow{S}$ as a vector product of $\overrightarrow{E}$ and $\overrightarrow{H}$; therefore, a fixed relationship between the power-radiation density $\overrightarrow{S}$, interconnected electric field $\overrightarrow{E}$, and magnetic field $\overrightarrow{H}$ can be illustrated in Fig. 5 and presented in (2) and (3),
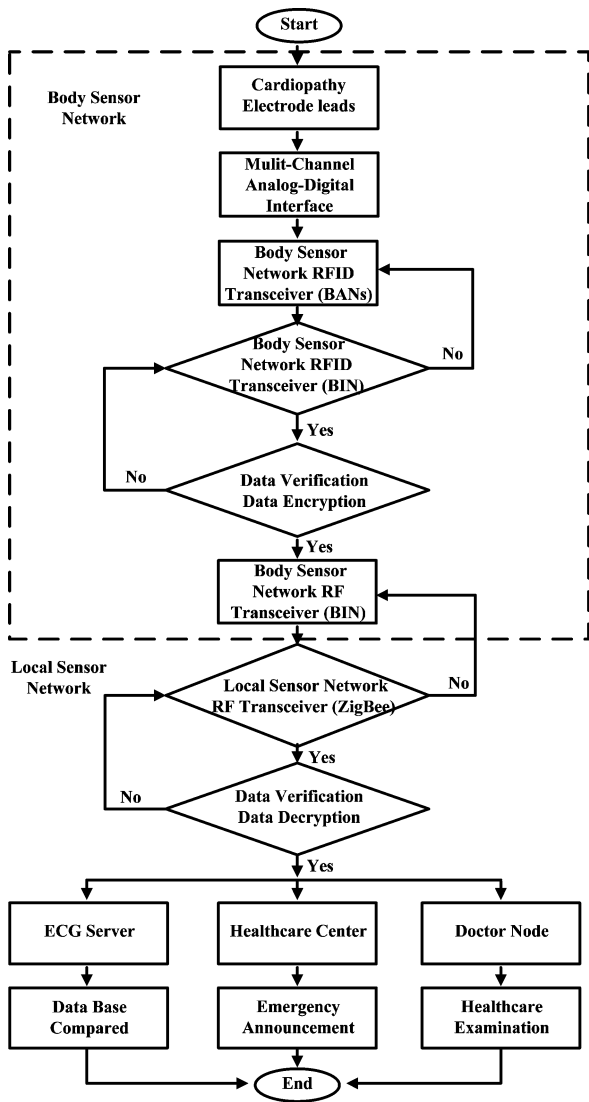
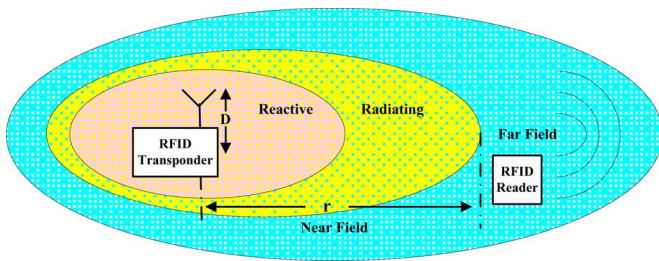Fig. 2.　Data flowchart for the ECG detection.

Fig. 3.　Antenna in near-field and far-field regions.

respectively [19]

$$\vec{S} = \vec{E} \times \vec{H} \tag{2}$$

$$\vec{E} = \vec{H} \cdot \sqrt{\frac{\mu_0}{\varepsilon_0}} = \vec{H} \cdot Z_F \tag{3}$$

where the vacuum permeability and permittivity of the free-space propagation medium in the EM wave are μ_0 and ε_0, respectively, and the Z_F is the characteristic wave impedance
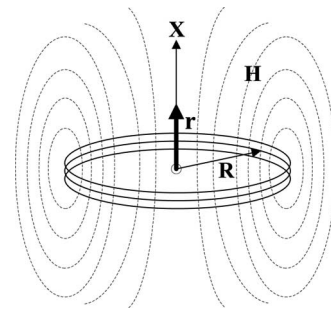

Fig. 4.　Path of the lines of magnetic flux around a short round coil.
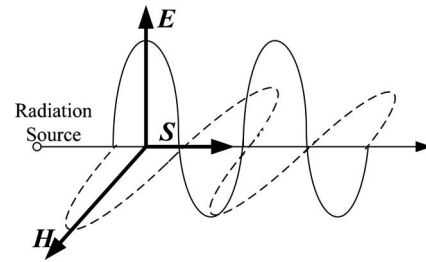

Fig. 5.　Poynting radiation vector $\vec{S}$ as the vector product of $\vec{E}$ and $\vec{H}$.
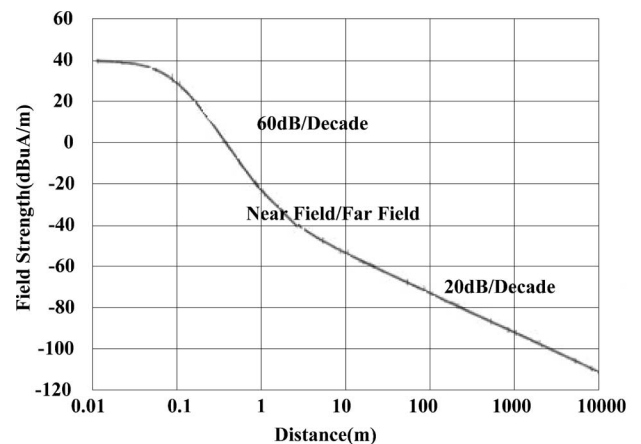

Fig. 6.　Magnetic field strength H versus distance in the near field and the far field.

in the free space. Therefore, the electric field strength E at a certain distance r from the radiation source can be calculated by (4), where P_{EIRP} is the transmission power emitted from the isotropic emitter

$$\vec{E} = \sqrt{\frac{P_{\text{EIRP}} \times Z_F}{4\pi r^2}}. \tag{4}$$

The fields are unique and irrelevant mutually, and the propagation microwave attenuation via free-space impedance is only decayed by $1/r$.

Fig. 6 shows the magnetic field strength versus distance in both the near field and the far field under the 13.56-MHz HF band. Field strength H through the radiation antenna will be operated in the near field, if it has a damping of 60 dB/decade of distance. Approaching the far field, the free-space attenuation

TABLE II
WAVELENGTH (λ) AND BOUNDARY (r) IN RFID SYSTEM

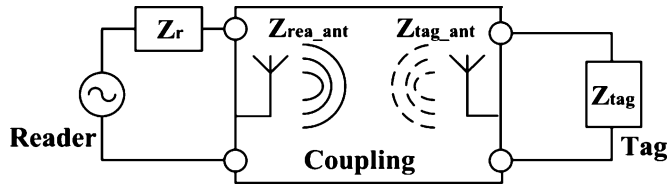| f (MHz)	λ (cm)	r (cm)	Band
0.125	240000	38197	LF
13.56	2212.39	352.11	HF
433	69.28	11.03	UHF
868	34.56	5.05	UHF
915	32.79	5.22	UHF
2450	12.24	1.95	Microwave

Fig. 7.   Two-port network model of power transmission.

of the EM waves in the field-strength path is only a damping of 20 dB/decade of distance.

The boundary between the near field and far field can be approximated and illustrated as $r = \lambda/2\pi$, where λ is the wavelength, which is usually larger than the antenna dimension. Table II shows the wavelength and boundary of different frequency bands. The boundary of the UHF bands is smaller than that of the HF and LF bands. Therefore, the UHF band is better for the biosignal transmission with longer distance communication.

B. RFID Power Transmission

Since the antenna dimension and transmission gain will affect system stability and data-transmission accuracy, the pattern should be carefully selected. In the RFID system, the patch antenna is preferred for use in a reader (BIN), while the dipole antenna [17] is commonly adopted in a transponder (BAN). Moreover, the antenna dimension is dependent on the wavelength and the power-transmission gain, thus the dimension can be decreased under the higher operated frequency and lower transmission gains. Therefore, in this study, the UHF with 915 MHz is employed in the RFID power transmission and physical design.

The power transmission between the UHF reader's and transponder's antenna can be represented by a well-known linear two-port network model, as shown in Fig. 7, where $Z_r = R_r + jX_r$ is the output impedance (typically 50 Ω) of the reader, $Z_{\text{rea\_ant}} = R_t + jX_t$ is the transmitted antenna impedance of the reader, $Z_{\text{tag\_ant}} = R_a + jX_a$ is the received antenna impedance of the transponder, and $Z_{\text{tag}} = R_c + jX_c$ is the chip input impedance of the transponder [18].
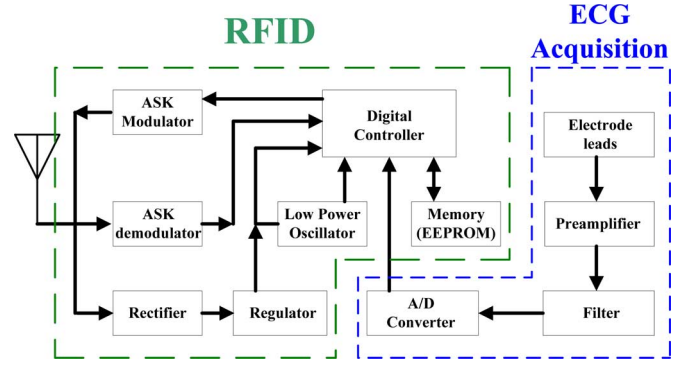

Fig. 8.   Proposed block diagram in a BAN.

To assess the available energy of a transponder, the free-space attenuation a_F relative to the distance r of the antenna between the reader and the transponder, as illustrated in (5) [19], can be estimated, where G_{tag} and G_{rea} are the transmission antenna gains of the transponder and reader, respectively, and f is the transmission frequency of the reader. Moreover, the power received by the transponder's antenna can be obtained by (6), where P_{tag} is the received power of the transponder and P_{rea} is the transmitted power of the reader

$$a_F = -147.6 + 20\log(r) + 20\log(f) - G_{\text{rea}} - G_{\text{tag}} \quad (5)$$

$$P_{\text{tag}} = \frac{P_{\text{rea}}}{10^{a_F/10}}. \quad (6)$$

Based on our design, given the distance r of 1 m and the transmission frequency f of 915 MHz, the implemented impedances of the reader, the patch antenna, and the long dipole antenna are 50, 42, and 73 Ω, respectively, and the measured antenna gains of a reader G_{rea} and a transponder G_{tag} are 2 and 1.6 dBi, respectively. Therefore, if the effective isotropic radiated power (EIRP) of the reader's antenna is 70 mW, the attenuation a_F is 28.03 dB in the 1-m free space between the reader and the transponder, if we use (5) and (6), while the effectively received power in the transponder received antenna is 0.25 mW. The effectively received power will provide the supply voltage for the ICs in the transponder without a battery. Equation (7) can be used to calculate the received equivalent voltage of 0.36 V with P_{tag} of 0.25 mW and R_{ant} of 73 Ω

$$V_{\text{RF}} = 2\sqrt{2} \times \sqrt{P_{\text{tag}} \times R_{\text{ant}}}. \quad (7)$$

IV. PASSIVE RFID TRANSPONDER AND CIRCUIT IMPLEMENTATION OF THE ECG ACQUISITION SYSTEM

In Fig. 1, a BAN consists of an RFID transponder and an ECG acquisition system (see Fig. 8). Since the received power from the reader in the BIN is small, as described in the previous section, a rectifier with a charge pump and a regulator with pure dc-output voltage are required to provide the voltage supply for the ICs in a BAN. Moreover, the basic communication ICs and analog front-end circuits shown in Fig. 8 are also required to achieve the biosignal acquisition and wireless communication. To ensure that the whole circuit is performed in normal operation under the low received power, the required ICs in a BAN should
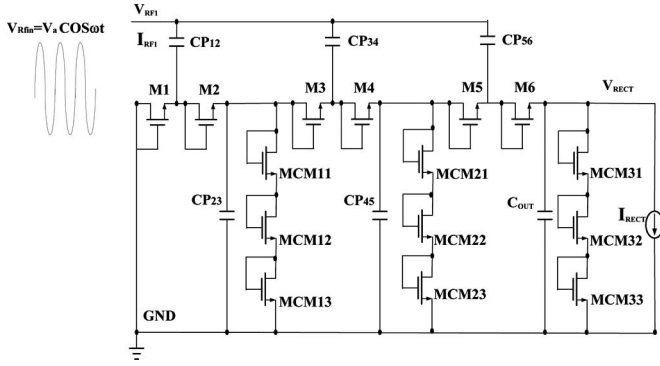
Fig. 9.   Rectifier with charge pump circuit.

be implemented in low-power consumption. The detailed low-power circuits are described in this section and how they fit the power specification in a BAN is demonstrated.

A. Rectifier With Charge Pump

A proposed rectifier, as shown in Fig. 9, is employed in the dc-voltage-supply generation from the received EM field. The received root-mean-square voltage (V_{RF1}) and current (I_{RF1}) at the input are 0.36 V and 552 μA, respectively, as derived by (7) under the distance of 1 m between the BIN and BANs. This voltage is not appropriate for the operation of ICs implemented in the 0.18-μm CMOS process with a threshold voltage of 0.5 V. Therefore, the charge pump circuit should be integrated in the rectifier to pump the voltage from 0.36 V to near 1 V in the worst case [20], [21]. As shown in Fig. 9, the diode-connected transistors (M_i) with capacitors (CP_i) can be adopted to implement the rectifier circuit capable of rectification and can serve as the voltage pump, simultaneously. However, to prevent the over-pump voltage from destroying the active circuits, the clamped transistors (MCM$_i$) are also employed to suppress the output voltage of the rectifier.

According to the simulation under V_{RF1} of 0.36 V and I_{RF1} of 552 μA, the output voltage V_{RECT} and current I_{RECT} of the rectifier are 1.2 V and 59 μA, respectively. The PCE defined in (8) can achieve 36%, which is higher as compared to the conventional rectifier with a PCE of 5% [20]. The estimated time constant (τ_{RECT}) of rectifier with charge pump circuit is 3.64 μS to achieve less than 0.1% error, according to (9), where R_{req} and C_{Load} are Thevenin's equivalent output resistance and equivalent load capacitance of charge pump circuit, respectively

$$\text{PCE} = \frac{P_{\text{out}}}{P_{\text{in}}} = \frac{I_{RECT}(\text{rms})V_{RECT}(\text{rms})}{I_{RF1}(\text{rms})V_{RF1}(\text{rms})} \qquad (8)$$

$$\tau_{RECT} = 7R_{req}C_{Load} = 7\frac{V_{RECT(\text{rms})}}{I_{RECT(\text{rms})}}C_{Load}. \qquad (9)$$

B. Regulator Circuit

The regulator circuit does not only regulate the output voltage of the rectifier to a stable dc, but also provides protection behind the ICs against higher RF input power due to the short distance coupling between the BIN and BANs. The implemented regu-
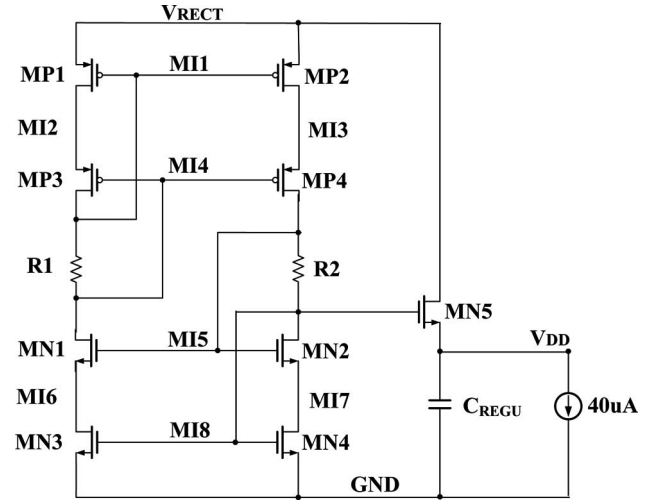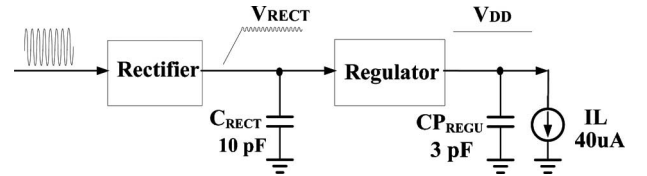

Fig. 10.   Regulator circuit.

Fig. 11.   Block diagram of power transformation.

lator circuit with a bandgap reference structure is illustrated in Fig. 10, which is combined with the proposed rectifier, as shown in Fig. 11, to verify the ac-to-dc converter.

According to the simulation results under a distance coupling of 1 m, the regulator output voltage V_{DD} is 0.87 V, while the power consumption of the ac-to-dc converter is 41.76 μW. The estimated time constant (τ_{REGU}) of regulator is 1.1 μS to achieve less than 10% error calculated by (10), where R_{req} and C_{REGU} are Thevenin's equivalent output resistance and output load capacitance of regulator, respectively. The simulated total time constant is 4.81 μS from the RF reading signal to stable dc-output voltage

$$\tau_{REGU} = 2.3R_{req}C_{REGU} = \frac{V_{DD}}{I_{DD}}C_{REGU}. \qquad (10)$$

C. Low-Power Oscillator Circuit

In the RFID transponder, a clock is required to enable the analog and digital circuits, such as encoder/decoder, encryption/decryption, synchronization, and switched-capacitor circuits. For the implantable wireless communication system, the clock can be directly extracted from the RF input signal with carrier frequency of 2 MHz [10]. However, because the carrier frequency in the body sensor network with UHF is rather high, e.g., 915 MHz and the extracted clock should be divided into an LF for system requirement; the extracted circuits and dividers usually consume more power. Therefore, a low-power internal clock is required. As shown in Fig. 12, a ring oscillator with nine-stage inverters, a buffer with three-stage inverters, and a divider with a D flip-flop are implemented to generate the
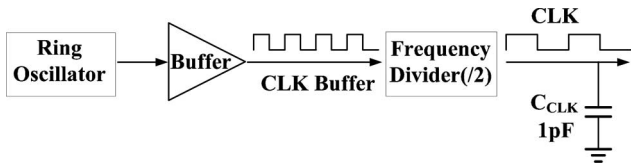
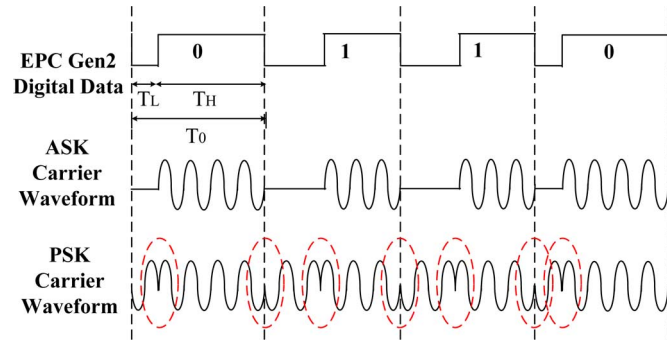Fig. 12. Clock generator for internal system clock.

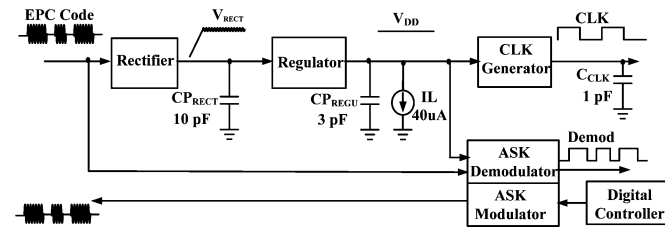Fig. 13. ASK and PSK waveform employed in digital modulation.

Fig. 14. RF front-end block in a BAN.

(a)

(b)

Fig. 15. (a) ASK demodulator and (b) ASK modulator with class-E amplifier.

a full modulation index with an ON–OFF keying is used here. In addition, the output match network is required to achieve maximum output power at the dipole antenna.

E. Digital Controller and EEPROM Memory

1) Digital Controller: A 15-bit protocol, as shown in Fig. 16(a), is used in the digital controller to control the received data and process the transmitted data. It comprises of two start bits and two stop bits for recognizing the command, three address bits for channel selection for placing electrodes in the transverse plan under the ECG measurement, and eight data bits for processing the encryption and decryption. All the data are stored in the electrically erasable ROM (EEROM) memory. The hardwares of encryption and decryption will dominate the power consumption of digital system. Based on the chaos theory [24], a low-power encryption/decryption system is proposed to estimate the power feasibly. Fig. 16(b) and (c) shows the hardware architectures of encryption and decryption, respectively. A real-time-logic (RTL) coding method is employed to synthesize the hardware with the 0.18-μm CMOS technology. According to the simulation result, the power consumption of both encryption and decryption are 16.9 and 19.3 μW, respectively.

2) Electrically-Erasable Programmable Read-Only Memory (EEPROM): The silicon-based nonvolatile memory EEPROM retains data without consuming power, and the data retention is usually 30 years at the minimum. The power estimation of the EEPROM is based on the memory size of 1.3 kb [25], which is enough to store the personal identification and command word, and the estimated result is 10 μW.

required system clock of 100 kHz. According to the simulation results, the power consumption of the whole circuit is 10.4 μW only.

D. ASK Demodulator/Modulator Circuit

Most of the digital modulations employed in RFID application are the ASK and the PSK. Fig. 13 illustrates the Electronic Product Code Generation 2 (EPC Gen2) digital data in RFID handbook [19] versus the ASK and PSK modulation. In general, the ASK modulation is commonly used in RFID communications and biomedical systems [21], especially in UHF band for simple design and low-power concerns [22].

Fig. 14 depicts the RF front-end block and the required ASK demodulator/modulator circuits (see Fig. 15). The ASK demodulator in the receiver of a BAN consists of an envelop detector, a low-pass filter, and a comparator with an output buffer. The envelop detector is a half-wave rectifier used to detect the positive waveform and the low-pass filter is employed to average the noise and to extract the envelope signal. The comparator with a threshold voltage of 0.45 V is used to precisely detect the digital data. According to the simulation result, the power consumption is only 9.3 μW.

The ASK modulator in the transmitter of the BAN can be combined with a class-E amplifier [23], as shown in Fig. 15(b) to modulate the digital signal. For easier data discrimination,
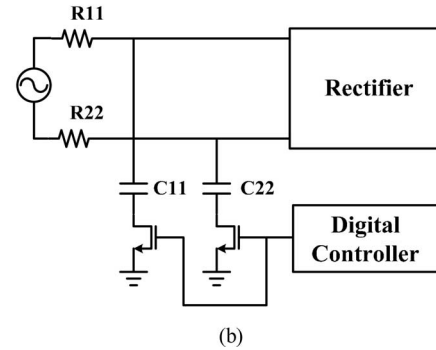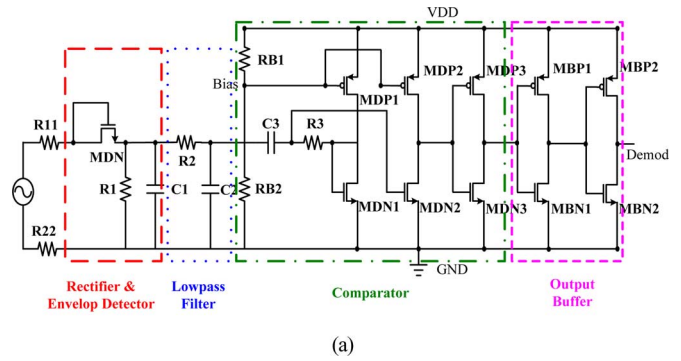
(a)

(b)

(c)
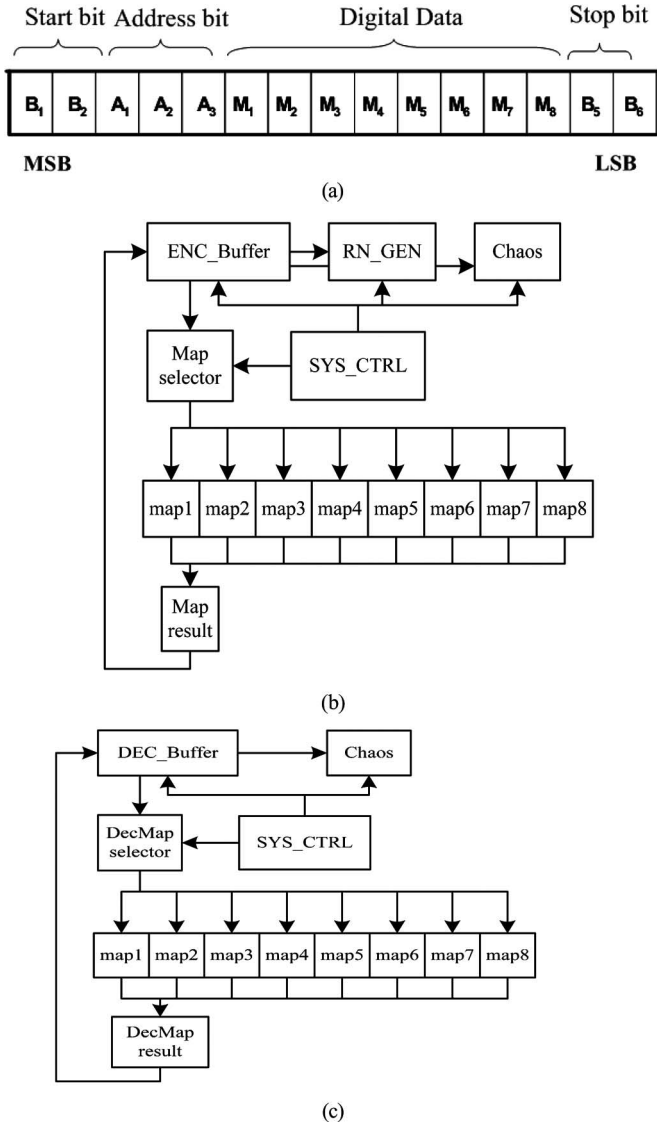
Fig. 16. (a) Format of the 15-bit command word. Hardware architecture of (b) encryption and (c) decryption.

Fig. 17.   Proposed VGA with an AGC.

Fig. 18.   Low-power fifth-order Butterworth filter with the cutoff frequency of 250 Hz.

F. ECG Acquisition System

The ECG acquisition system in a BAN is responsible for processing the ECG signal sensing from the electrode leads and transmitting it to the BIN for recording and analysis. This ECG signal detected by the electrode leads is a weak signal with an amplitude range of 100 μV–4 mV [26] and includes some noise resulting from the 60-Hz power lines and instrument interference. Therefore, a preamplifier and a filter were required to clarify the signal before using the ADC. The detailed circuit components are as follows.

1) Preamplifier: A variable gain amplifier (VGA) with automatic gain control (AGC) circuits composed of a peak detector (PD), and a nonlinear controller (NC) for digital ECG [27], as shown in Fig. 17, was adopted to estimate the power consumption feasibly. The proposed amplifier is a feedback system: VGA is used to compress (or amplify) the signal. The peak value of the VGA output would be detected by the PD and compared
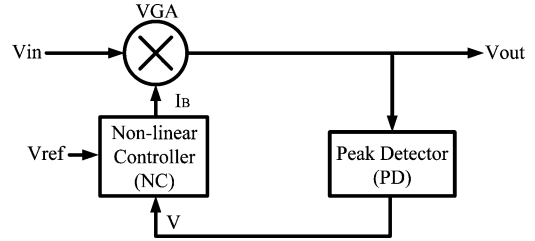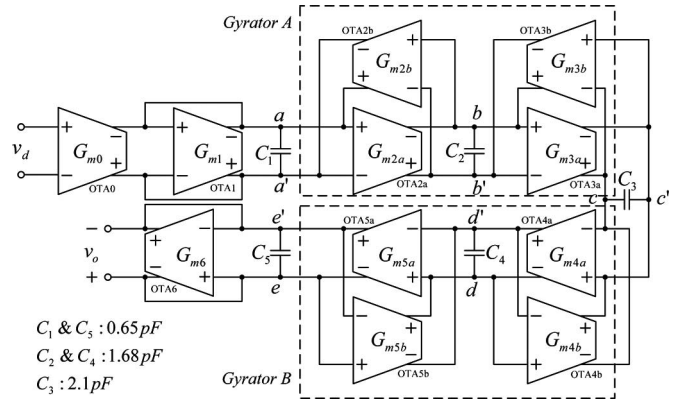
with the reference voltage ($V_{\rm ref}$) by the NC to control the operation of VGA. According to the simulation results, the maximum gain range of the AGC amplifier was 52 dB, and the power consumption was only 1.8 μW under the normal operation, and the SNR was 39 dB.

2) Low-Pass Filter: To preprocess the ECG signal, an ultralow power filter behind the preamplifier was required to decrease the out-of-band noise. Therefore, a fifth-order Butterworth filter, as shown in Fig. 18, was adopted [26] to realize the low-pass filter with the cutoff frequency of 250 Hz. The in-band performance of the fifth-order Butterworth filter was good enough to filter the out-of-band noise and restore the ECG signal precisely. This circuit was verified by the measurement result, which reveals that it had a dynamic range of 50 dB and a power consumption of 452 nW under 1-V supply voltage.

3) AD Converter: ADCs were required for processing analog ECG signals in the digital domain. A low-power successive approximation (SA) ADC with an 8-bit resolution and 10-kHz sampling frequency was designed [28] to meet the requirement of ECG acquisition systems. The basic architecture of an SA ADC is illustrated in Fig. 19. The converter consists of an S/H circuit, a comparator, a SA register (SAR) controller, and an 8-bit digital-to-analog converter (DAC). Using a binary searching algorithm, the input sample voltage can be successively approximated by the DAC output voltage. The subthreshold technique was adopted in the comparator design to decrease the power consumption of the SA ADC. Meanwhile, a passive S/H circuit and an opamp-free, capacitor-based DAC were likewise used to meet the low-power requirement. According to the measurement results, the signal-to-noise distortion ratio (SNDR)
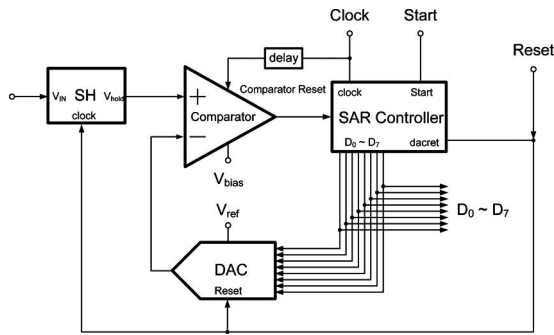
Fig. 19.   Block diagram of an SA ADC.

TABLE III
POWER BUDGET FROM BIN TO BANs AND THE POWER
CONSUMPTION OF ICs IN A BAN

Operation Frequency	915 MHz
Reading Distance	1 m
Reader Antenna Radiation Power	70mW
Dipole Antenna Received	252µW (-10dBm)
Rectifier Power Conversion Efficiency	36%
Transponder Provided Power	100.8 µW
Regulator Power consumption	41.76 µW
ASK Demodulator Power	9.3 µW
CLK Power	10.4 µW
Maximum Digital Power	19.3 µW
Memory Power	10 µW
A/D Converter	0.95µW
Filter	0.453µW
Preamplifier	1.5µW
Estimated ICs Power in Transponder	93.66µW

was 45.2 dB, and the peak spurious free dynamic range (SFDR) was 54 dB. The effective number of bits (ENOB) was 7.2 bits and its differential nonlinearity (DNL) and integral nonlinearity (INL) were $-0.41/+0.38$ and $-0.89/+0.6$ LSB, respectively. Moreover, the power consumption of this 8-bit SA ADCs was 0.95 μW.

V.   CONCLUSION

This paper has presented heterogeneous networks, including a body sensor network and a local sensor network for healthcare monitoring. For miniaturization and SOC concerns, the RFID field analysis in the body sensor network was discussed and the required ICs in BANs were designed to estimate the power budget and feasibility in the implementation. Table III shows the power budget under the design. According to the simulation and the measurement results, the ICs can fit in with the link budget in the UHF RFID system under the 1-m communication distance that is compatible with the body sensor network. The proposed

ICs will be fabricated in TSMC 0.18-μm CMOS process in the future.

REFERENCES

[1] S. W. Wang, W. H. Chen, C. S. Ong, L. Liu, and Y. W. Chuang, "RFID applications in hospital: a case study on a demonstration RFID project in Taiwan hospital," in *Proc. 39th Hawaii Int. Conf. Syst. Sci.*, 2006, pp. 184a–184a.
[2] A. Lahtela, M. Hassinen, and V. Jylha, "RFID and NFC in healthcare: Safety of hospital medication care," in *Proc. Second Int. Conf. Pervasive Comput. Technol. Healthcare*, 2008, pp. 241–244.
[3] S. L. Garfinkel, A. Juels, and R. Pappu, "RFID privacy: An overview of problems and proposed solutions," *IEEE Security Privacy*, vol. 3, no. 3, pp. 34–43, May/Jun. 2005.
[4] H. H. Asada, P. Shaltis, A. Reisner, S. Rhee, and R. C. Hutchinson, "Mobile monitoring with wearable photoplethysmographic biosensor," *IEEE Eng. Med. Biol. Mag.*, vol. 22, no. 3, pp. 28–40, May/Jun. 2003.
[5] E. Jovanov, D. Raskovic, J. Price, A. Moore, J. Chapman, and A. Krishnamurthy, "Patient monitoring using personal area networks of wireless intelligent sensors," *Biomed. Sci. Instrum.*, vol. 37, no. 12, pp. 373–378, Dec. 2001.
[6] M. D. Rodriguez, J. Favela, E. A. Martinez, and M. A. Munoz, "Location-aware access to hospital information and services," *IEEE Trans. Inf. Technol. Biomed.*, vol. 8, no. 4, pp. 448–455, Dec. 2004.
[7] K. Lorincz, D. J. Malan, T. R. F. Fulford-Jones, A. Nawoj, A. Clavel, V. Shnayder, G. Mainland, M. Welsh, and S. Moulton, "Sensor networks for emergency response: Challenges and opportunities," *Pervasive Comput.*, vol. 3, no. 4, pp. 16–23, Oct.–Dec. 2004.
[8] C. S. Pattichis, E. Kyriacou, S. Voskarides, M. S. Pattichis, R. Istepanian, and C. N. Schizas, "Wireless telemedicine systems: An overview," *IEEE Antennas Propag. Mag.*, vol. 44, no. 2, pp. 143–153, Apr. 2002.
[9] P. E. Ross, "Managing care through the air," *IEEE Spectr.*, vol. 41, no. 12, pp. 26–31, Dec. 2004.
[10] S. Y. Lee and S. C. Lee, "An implantable wireless bidirectional communication microstimulator for neuromuscular stimulation," *IEEE Trans. Circuits Syst. I, Reg. Papers*, vol. 52, no. 12, pp. 2526–2538, Dec. 2005.
[11] C. C. Lin, P. Y. Lin, P. K. Lu, C. Y. Hsieh, W. L. Lee, and R. G. Lee, "A healthcare integration system for disease assessment and safety monitoring of dementia patients," *IEEE Trans. Inf. Technol. Biomed.*, vol. 12, no. 5, pp. 579–586, Sep. 2008.
[12] ZigBee Alliance (2007, Oct.). [Online]. Available: http://www.ZigBee.org
[13] *IEEE Standard 802.15.4: Wireless Medium Access Control (MAC) and Physical Layer (PHY) Specification for Wireless Personal Area Networks (WPANs)*, IEEE Standard Part 15.4, 2003.
[14] J. Ayoade, "Security implications in RFID and authentication processing framework," *Comput. Security*, vol. 25, no. 3, pp. 207–212, May 2006.
[15] A. Juels, "RFID security and privacy: A research survey," *IEEE J. Sel. Areas Commun.*, vol. 24, no. 2, pp. 381–394, Feb. 2006.
[16] P. V. Nikitin, K. V. S. Rao, and S. Lazar, "An overview of near field UHF RFID," in *Proc. IEEE Int. Conf. RFID*, 2007, pp. 167–174.
[17] J. D. Kraus and R. J. Marhefka, *Antennas for All Application*, 2nd ed. New York: McGraw-Hill, 2001.
[18] P. V. Nikitin, K. V. S. Rao, S. F. Lam, V. Pillai, R. Martinez, and H. Heinrich, "Power reflection coefficient analysis for complex impedances in RFID tag design," *IEEE Trans. Microw. Theory Tech.*, vol. 53, no. 9, pp. 2721–2725, Sep. 2005.
[19] K. Finkenzeller, *RFID Handbook*, 2nd ed.   New York: Wiley, 2003.
[20] E. Bergeret, J. Gaubert, P. Pannier, and J. M. Gaultier, "Modeling and design of CMOS UHF voltage multiplier for RFID in an EEPROM compatible process," *IEEE Trans. Circuits Syst. II, Exp. Briefs*, vol. 54, no. 10, pp. 833–837, Oct. 2007.
[21] S. Chiu, I. Kipnis, M. Loyer, J. Rapp, D. Westberg, J. Johansson, and P. Johansson, "A 900 MHz RFID reader transceiver IC," *IEEE J. Solid-State Circuits*, vol. 42, no. 12, pp. 2822–2833, Dec. 2007.
[22] U. Karthaus and M. Fischer, "Fully integrated passive UHF RFID transponder IC with 16.7-μ/W minimum RF input power," *IEEE J. Solid-State Circuits*, vol. 38, no. 10, pp. 1602–1608, Oct. 2003.
[23] G. A. Kendir, W. Liu, G. Wang, M. Sivaprakasam, R. Bashirullah, M. S. Humayun, and J. D. Weiland, "An optimal design methodology for inductive power link with class-E amplifier," *IEEE Trans. Circuits Syst. I, Reg. Papers*, vol. 52, no. 5, pp. 857–866, May 2005.
[24] J. C. Yen and J. I. Guo, "Design of a new signal security system," in *Proc. IEEE Int. Symp. Circuits Syst.*, May 2002, pp. 121–124.

[25] ATMEL Corp., *1.3-kbits UHF R/W IDIC With Anti-Collision Function*, ATA5590 Datasheet, Sep. 2004.

[26] S. Y. Lee and C. J. Cheng, "System design and modeling of a OTA-C filter for portable ECG detection," *IEEE Trans. Biomed. Circuits Syst.*, vol. 3, no. 1, pp. 53–64, Feb. 2008.

[27] Y. C. Su, S. Y. Lee, and A. P. Lin, "A 0.6-V 1.8-μW automatic gain control circuit for digital hearing aid," in *Proc. IEEE Asia Pac. Conf. Circuit Syst.*, Dec. 2008, pp. 113–116.

[28] S. Y. Lee, C. J. Cheng, S. C. Lee, and K. M. Huang, "A 1-V 8-bit 0.95uW successive approximation ADC for biosignal acquisition systems," in *Proc. IEEE Int. Symp. Circuits Syst.*, May 2009, pp. 649–652.

Liang-Hung Wang (S'08) was born in Tainan, Taiwan, in 1976. He received the B.S. and M.S. degrees in electronic engineering from I-Shou University, Kaohsiung, Taiwan, in 2000 and 2003, respectively. He is currently working toward the Ph.D. degree from the Institute of Electrical Engineering, National Chung Cheng University, Chia-Yi, Taiwan.

His current research interests include the low-power and low-voltage active radio-frequency (RF) front-end integrated circuits, passive RF identification analog circuits for biomedical application, and baseband system for wireless communications.

Shuenn-Yuh Lee (M'98) was born in Taichung, Taiwan, in 1966. He received the B.S. degree from National Taiwan Ocean University, Chilung, Taiwan, in 1988, and the M.S. and Ph.D. degrees from National Cheng Kung University, Tainan, Taiwan, in 1994 and 1999, respectively.

In 2002, he was an Assistant Professor at the Institute of Electrical Engineering, National Chung Cheng University, Chia-Yi, Taiwan, where he has been an Associate Professor since 2006. His current resea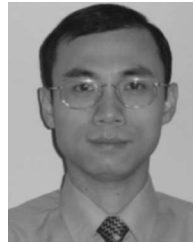rch interests include design of analog and mixed-signal integrated circuits (ICs), including filter, high-speed analog-to-digital converter (ADC)/digital-to-analog convertor (DAC), and sigma–delta ADC/DAC, biomedical circuits and systems, low-power and low-voltage analog circuits, and radio-frequency front-end integrated circuits for wireless communications.

Dr. Lee is currently a member of the Circuits and Systems Society, the Solid-State Circuits Society, Medicine and Biology Society, and the Communication Society of the IEEE. He is also a member of the Institute of Electronics, Information, and Communication Engineers and the Chinese Institute of Electrical Engineering. He is also the Chairman of the Heterogeneous Integration Consortium sponsored by the Ministry of Education, Taiwan to serve the education on IC design of Taiwan.

Qiang Fang (M'98) received the B.S. degree in applied physics from Tsinghua University, Beijing, China in 1991, and the Ph.D. degree in biomedical engineering from Monash University, Clayton, Vic., Australia, in 2000.

In 2000, he joined Royal Melbourne Institute of Technology, Melbourne, Vic., Australia, where he is currently a Senior Lecturer in the School of Electrical and Computer Engineering. His research interests include intelligent and miniaturized medical instrumentation, wearable and implantable body sensor network, and pervasive computing technologies applicable to healthcare delivery.